Direct Deposition of Aligned Single Walled Carbon Nanotubes by Fountain Pen Nanolithography

Materials Express

2158-5849/2011/1/279/006
doi:10.1166/mex.2011.1044
www.aspbs.com/mex

Direct Deposition of Aligned Single Walled Carbon Nanotubes by Fountain Pen Nanolithography

Kirsten M. Strain[1], Talia Yeshua[2], Andrei V. Gromov[1], Oleg Nerushev[1], Aaron Lewis[2], and Eleanor E. B. Campbell[1,3,*]

[1]*EaStCHEM, School of Chemistry, Edinburgh University, Edinburgh EH9 3JJ, Scotland*
[2]*Department of Applied Physics, Hebrew University of Jerusalem, Jerusalem 91904, Israel*
[3]*Division of Quantum Phases and Devices, School of Physics, Konkuk University, Seoul 143-701, Korea*

Fountain pen nanolithography was used to deposit controllably nanotube dispersions on a silicon substrate with high spatial precision. The deposited structures were analysed using atomic force microscopy, scanning electron microscopy and polarised Raman spectroscopy. The Raman spectroscopy showed that the deposited nanotubes had a very high degree of alignment with around 90% of the nanotubes aligned at an angle less than 30 ° from the direction of writing.

Keywords: Carbon Nanotubes, Fountain Pen Nanolithography, Polarised Raman Spectroscopy, Aligned Deposition.

1. INTRODUCTION

The integration of single walled carbon nanotubes (SWNTs) into nanoelectrical devices is an important area in the field of nanotechnology. However, challenges remain in fabricating devices containing carbon nanotubes. Growing SWNTs on a substrate then lithographically patterning electrodes and other device features onto the substrate, can remove or contaminate the SWNTs. On the other hand, fabricating all the other device features first and then growing or depositing SWNTs has other drawbacks. For most post-fabrication growth techniques, the device is exposed to high temperatures, which limits the materials which can be used. If post-fabrication deposition of pre-grown carbon nanotubes is to be used then the challenge is in placing SWNTs in the desired location.

*Author to whom correspondence should be addressed.
Email: eleanor.campbell@ed.ac.uk

The most common method of such placement of carbon nanotubes in specific spatial positions to date is dielectrophoresis,[1] whereby the application of an ac bias between pre-patterned electrodes creates an inhomogeneous electric field with the nanotubes being attracted to the region of highest field. While careful application of this technique can give good results, even allowing the placement of an individual SWNT between two electrodes,[2] works preferentially for metallic nanotubes. In addition, the specific electrode arrangement required to apply the electric field may interfere with the desired final structure. The need for a method of placing both metallic and semiconducting SWNTs from dispersion onto substrates with no special electrode arrangement leaves the field searching for new deposition techniques.

Fountain pen nanolithography (FPN) is a deposition technique where material is applied to a surface through a nanopipette in contact with the surface. The technique was first used by Lewis et al.[3] to apply a chemical etchant to a chrome surface through a micropipette held in an atomic force microscope and since then has also been used to place proteins[4,5] and gold nanoparticles[6] in spatially precise locations on surfaces. While it is similar in concept to dip-pen nanolithography,[7] FPN has the advantage that a continual supply of material can flow to the tip, negating the need to leave the location of interest to pick up more material from a separate reservoir.

In this report, we apply the FPN technique to the deposition of SWNTs and, by use of polarised Raman spectroscopy, show that a high degree of alignment can be obtained.

2. EXPERIMENTAL DETAILS

Cantilevered quartz nanopipettes were used in the fountain pen nanolithography (FPN) method for the deposition of

SWNTs.[3] The cantilevered nanopipette is mounted on the tip holder in place of a standard tip in an atomic force microscope which allows control of the normal force by way of a beam-bounce feedback mechanism (Fig. 1). The aperture of the pipette was 150 nm.

The substrate used here was silicon, with a native oxide layer. A two-step piranha cleaning procedure was employed (98% H_2SO_4, 6 ml + 30% H_2O_2, 5 ml for 20 minutes at 90 °C followed by conc. NH_4OH, 1 ml + 30% H_2O_2, 1 ml + distilled H_2O, 5 ml for 15 minutes at 70 °C). The surface was then covered with a self-assembled monolayer of (3-aminopropyl) triethoxysilane (APTES) by immersion for 3 minutes in an aqueous solution of APTES. This chemical functionalisation affords the surface a greater affinity for carbon nanotubes than the unfunctionalised silica, causing the carbon nanotubes to 'stick' when they contact the surface. The surface was scratched with a diamond pen to create lines to act as location markers.

SWNTs (as produced HiPco[69] tubes from Carbon Nanotechnologies Inc., USA) were dispersed by horn ultrasonication in an aqueous solution of sodium dodecylbenzenesulfonate (SDBS) (0.2 mg/ml) then centrifugation, with a relative centrifugal force of ×20000 g, was performed for one hour to remove large bundles of carbon nanotubes. A drop of the supernatant was applied to the large-diameter end of the nanopipette and capillary forces drove it to the tip of the tapered end (Fig. 1).

The loaded nanopipette was placed inside an atomic force microscope (Nanonics MV1000, Nanonics Ltd. Israel). The approach of the pipette tip to the surface was monitored using a position-sensitive detector to measure the deflection of a laser reflecting off the top-side of the pipette. Tapping mode was used with a resonance frequency of 71 kHz and a setpoint of 80% of the total amplitude of vibration. When the tip made contact with the surface and was directed in a pattern, capillary action caused the dispersion of carbon nanotubes to be deposited, creating written lines. During this process the tip was moving at a speed of 10 μm s^{-1}, with small pauses at the corner points. The water quickly evaporated leaving SWNTs and SDBS in the written pattern. Imaging was done with a Veeco Nanoman VS with Dimension 3100 controller atomic force microscope (AFM) and a Hitachi 4700 II cold field-emission scanning electron microscope (SEM).

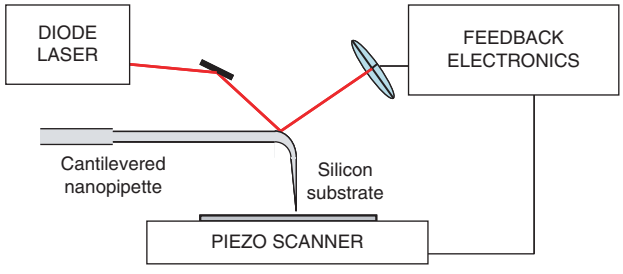

Fig. 1. Schematic diagram of cantilevered nanopipette used in place of an atomic force microscope tip. The laser provides feedback for maintaining constant force of contact.

Raman spectroscopy was performed on the deposited lines using a Renishaw inVia Reflex micro-Raman spectrometer with a 785 nm laser. The power density at the sample did not exceed 400 $\mu W \mu m^{-2}$. Polarised Raman spectroscopy was used to determine the degree of alignment of the SWNTs within the deposited lines. A schematic representation of the Raman microscope is shown in Figure 2. The incoming laser beam was passed through a $\lambda/2$ waveplate which could be rotated to give a range of incident laser polarisation directions on the sample. A polarising filter, placed in the scattered light path to act as an analyser, allowed the detector to measure the horizontally polarised scattered light. In addition, a second $\lambda/2$ waveplate could be placed before the analyser, allowing detection of the vertically polarised scattered light. Using this setup, two types of measurement were carried out. In the first case, the Raman intensity was mapped across the sample surface for two mutually orthogonal polarisation directions obtained with and without the two $\lambda/2$ waveplates in the beam path. In the second case, the incident polarisation direction was varied by rotating the first $\lambda/2$ waveplate. Then without and with the second $\lambda/2$ waveplate the horizontally and vertically polarised components

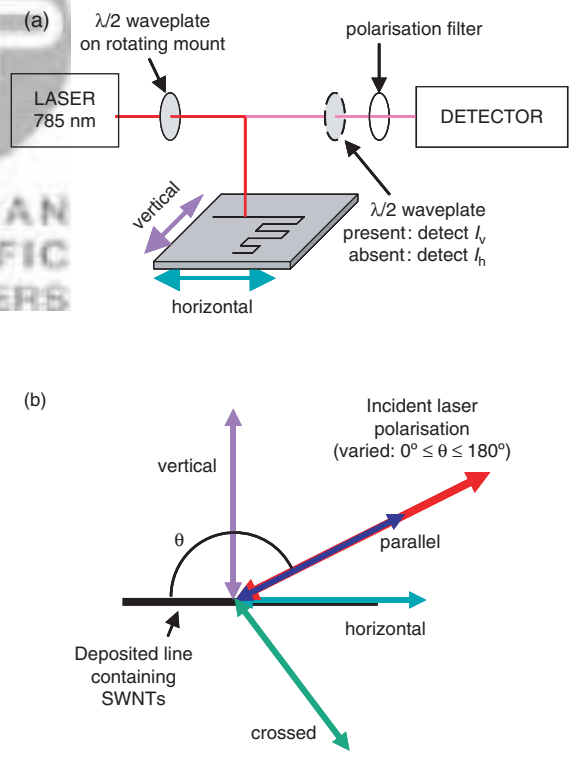

Fig. 2. (a) Diagram of Raman spectrometer detailing control of polarisation using two waveplates and a polariser giving horizontal and vertical components of scattered light and (b) relationship between horizontal and vertical and parallel and crossed polarisations, described in Eqs. (1) and (2). The sample is either crystalline calcium fluoride or the FPN-deposited SWNT-containing lines on a silicon substrate.

of the scattered light could be measured. The measurements of horizontally and vertically polarised light, I_h and I_v respectively, were then converted into measures of the scattered light polarised parallel, $I_\parallel$, and crossed, $I_\perp$, to the incident laser light as follows:

$$I_\parallel = I_h \cos^2\theta + I_v \sin^2\theta \quad (1)$$

$$I_\perp = I_h \sin^2\theta + I_v \cos^2\theta \quad (2)$$

where θ measures the angle between the polarisation of the laser line and the horizontal direction.

To take account of the influence the inherent polarisation dependence of the instrumentation has on the results, measurements were performed on the (111) surface of calcium fluoride. Its Raman peak at 322 cm^{-1} has a depolarisation ratio of 2/3 and a scattering efficiency that is independent of the laser polarisation's relation to the crystal axis.[8] Thus, when the measurements are taken at a range of polarisation angles as described above, the $I_\parallel$ and $I_\perp$ values should be independent of θ and the $I_\perp$ values should be 2/3 of the $I_\parallel$. Correcting the experimental data to reflect this for calcium fluoride gives a correction factor that can then be applied to the experimental data from the SWNT sample, eliminating the influence of polarisation-dependent laser intensity as well as the detection efficiency for different polarisations of scattered light.

3. RESULTS AND DISCUSSION

The AFM and SEM images of a pattern created by FPN using a SWNT dispersion are shown in Figures 3(a) and (b) respectively. Analysis of the dimensions measured by AFM shows an average height of 22 ± 18 nm and an average width (FWHM) of 800 ± 331 nm.

The presence of SWNTs was confirmed by Raman spectroscopy on one spot on the deposited line, which exhibited the characteristic *D* and *G* bands known for carbon nanotubes. A grid of 15 points was then mapped over the region of the deposited lines (Fig. 4(a)) and at each point two Raman spectra were measured. The first of these had the laser light polarised in the horizontal direction and the detector measuring the horizontally polarised scattered light, while the second used vertically polarised laser light and detecting the vertically polarised scattered light. As the sample was orientated with the deposited line in approximately the horizontal direction, this arrangement gave the parallel component of the scattered light in the approximate direction of the line and perpendicular to it. The Raman spectra obtained (examples given in Fig. 4(b)) were peak-fitted to measure the area of the *G* band. A correction factor from CaF_2 normalisation was applied to the measurements parallel to the written line and the results

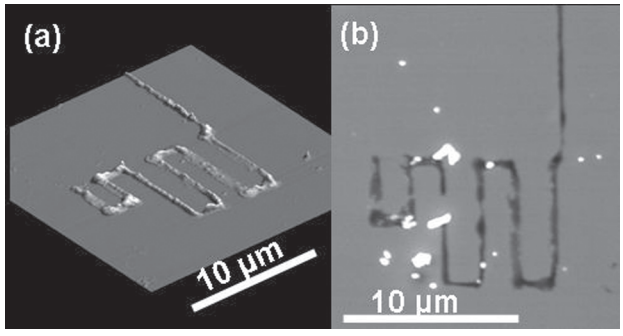

Fig. 3. (a) AFM and (b) SEM of pattern deposited by fountain pen nanolithography.

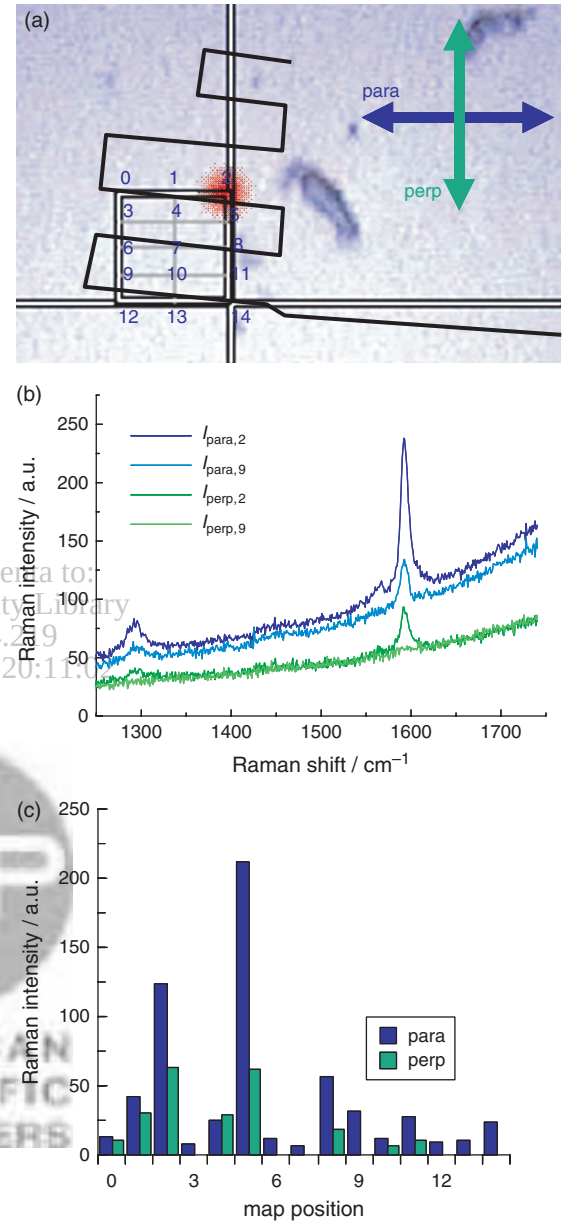

Fig. 4. (a) Optical microscope image showing grid where Raman spectra were taken and pattern of deposited lines superimposed from AFM data. (b) Sample Raman spectra from two points on the map. (c) Raman intensities measured parallel and perpendicular to the deposited line and normalised using CaF_2 calibration.

were plotted for each point in Figure 4(c). Note that some positions had too weak a signal in the perpendicular measurement to obtain a significant measurement. Clearly in most cases the parallel measurements are much stronger. As it is known that the Raman signal of an individual SWNT is strongest when the polarisation of the incident laser is parallel to the SWNT axis,[11] this is evidence that there is some degree of alignment of SWNTs within the deposited line throughout the deposited pattern.

The same FNP-deposited SWNT sample was then positioned in the Raman microscope such that the deposited line was aligned exactly parallel with the horizontal direction. The signal of the G band was measured with a range of laser polarisation directions, as described in the Methods section. The G band was peak-fitted with Lorentzian peaks and the height of the G^+ peak was taken as I_v or I_h. Equations (1) and (2) were used to convert to $I_\parallel$ and $I_\perp$, which were then corrected according to the CaF_2 normalisation and the results obtained are given in Figure 5.

To obtain quantitative information about the distribution of orientations of SWNTs in the deposited line, the analysis method of Liu and Kumar,[9] described by Perez et al.,[10] was applied. The following equation was applied to the experimental data for the parallel arrangement and the order parameters $\langle P_2(\cos\beta)\rangle$ and $\langle P_4(\cos\beta)\rangle$ were obtained from a least-squares fit, as shown in Figure 5.

$$\frac{I_\parallel(\theta)}{I_\parallel(\theta=0^\circ)} \propto \frac{\langle P_4(\cos\beta)\rangle[\cos^4\theta - 6/7\cos^2\theta + 3/35] + \langle P_2(\cos\beta)\rangle[6/7\cos^2\theta - 2/7] + 1/5}{\langle P_4(\cos\beta)\rangle 8/35 + \langle P_2(\cos\beta)\rangle 4/7 + 1/5} \quad (3)$$

The averaged Legendre polynomial, $\langle P_2(\cos\beta)\rangle$, is sometimes known as Herman's orientation parameter.[10] The angle β is the angle that a nanotube makes with respect to the deposited line direction. In completely random arrangements Herman's orientation parameter would have a value of 0 while in a system in which every SWNT was perfectly aligned with the $\theta = 0°$ direction its value would be 1. In the data given in Figure 5, the Herman's parameter value from the least-squares fit is 0.76.

Further information about the alignment of the SWNTs in the deposited line can be obtained by applying the principle of maximum information entropy to define an orientation distribution function (ODF), as discussed by Perez et al.[10] In general, the probability of finding a particle with orientations between angles (α, β, γ) and $(\alpha + d\alpha, \beta + d\beta, \gamma + d\gamma)$ is:

$$\int_{\lambda=0}^{\lambda=2\pi}\int_{\alpha=0}^{\alpha=2\pi}\int_{\beta=0}^{\beta=\pi} f(\alpha,\beta,\lambda)\sin\beta d\beta d\alpha d\gamma = 1 \quad (4)$$

where $f(\alpha, \beta, \gamma)$ is the ODF and α, β and γ are the Euler angles, with β defined as above. In the current system α may be disregarded as all of the SWNTs may be considered to be lying on the plane of the surface, in a two-dimensional arrangement. In addition, the cylindrical symmetry of SWNTs removes any dependence on γ. The ODF can then be written in an alternative form:

$$f(\beta) = A\exp[-(\lambda_2 P_2(\cos\beta)) + (\lambda_4 P_4(\cos\beta))] \quad (5)$$

where A is a constant and parameters λ_2 and λ_4 are Lagrange multipliers. The ODF is then known once these

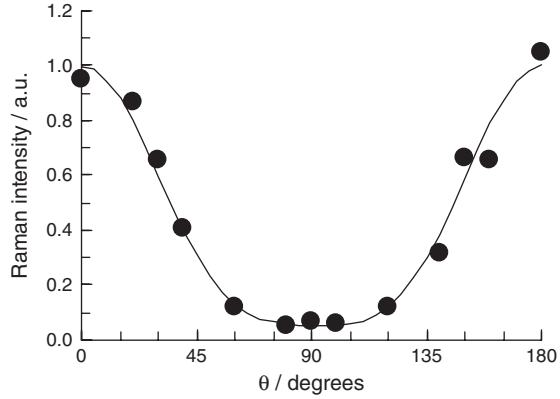

Fig. 5. Raman intensity as polarisation is rotated with respect to the deposited line orientation. The solid line represents a least-squares fit is based on Eq. (3).

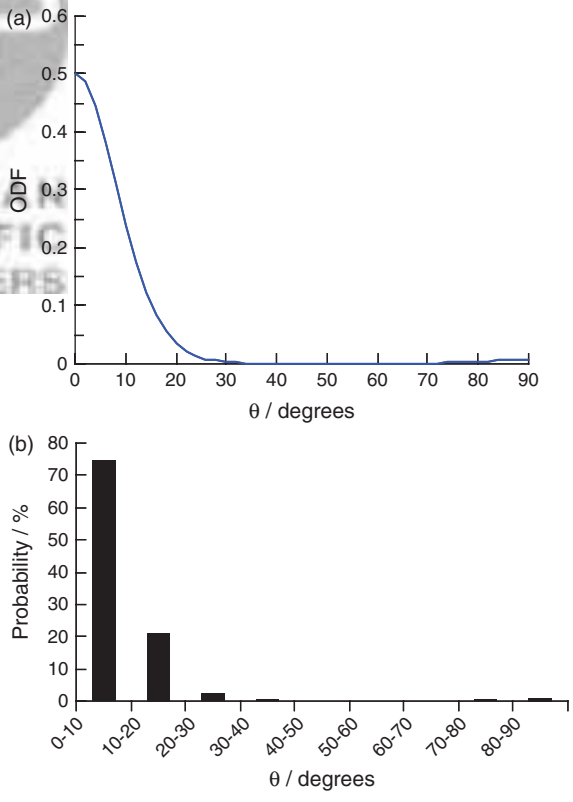

Fig. 6. (a) ODF and (b) histogram of probability of SWNT orientation in deposited line, based on Raman measurements in a parallel polarisation configuration.

Table I. ODF parameters obtained from repeated polarised Raman measurements on the SWNTs deposited by FPN.

Measurement	$\langle P_2(\cos\beta)\rangle^a$	$\langle P_4(\cos\beta)\rangle^a$	A^b	λ_2^b	λ_4^b	Abundance of SWNT within $-30° < \theta < 30°$ (%)
$1_\parallel$	0.76	0.70	0.0017	−0.91	−4.8	98
$1_\perp$	0.7	0.3	0.0015	−5.2	0.96	86
$2_\parallel$	0.68	0.24	0.00095	−6.2	1.8	82
$2_\perp$	0.67	0.37	0.0042	−2.8	−0.73	90
$3_\parallel$	0.68	0.42	0.0044	−2.5	−1.2	92
$3_\perp$	0.58	0.32	0.0061	−2.2	−0.84	86
$4_\parallel$	0.32	0.24	0.0098	−0.94	−1.3	76
$4_\perp$	0.56	0.13	0.0040	−3.6	1.0	74
$5_\parallel$	0.4	0.6	0.0059	−1.8	−1.5	90
$5_\perp$	0.6	0.2	0.0040	−3.5	0.55	80

[a]As defined in Eqs. (3) and (9) for parallel and perpendicular measurements, respectively. [b]As defined in Eq. (5).

three parameters are found, which can be done by numerically solving the following set of equations:

$$4\pi^2 \int_{\beta=0}^{\beta=\pi} f(\beta)\sin\beta\, d\beta = 1 \quad (6)$$

$$4\pi^2 \int_{\beta=0}^{\beta=\pi} P_2(\cos\beta) f(\beta)\sin\beta\, d\beta = \langle P_2(\cos\beta)\rangle \quad (7)$$

$$4\pi^2 \int_{\beta=0}^{\beta=\pi} P_4(\cos\beta) f(\beta)\sin\beta\, d\beta = \langle P_4(\cos\beta)\rangle \quad (8)$$

where $P_2(\cos\beta)$ and $P_4(\cos\beta)$ are Legendre polynomials or order of 2 and 4 respectively. The trapezoidal rule was used to solve these equations to obtain A, λ_2 and λ_4 by least-squares fit to the values of $\langle P_2(\cos\beta)\rangle$ and $\langle P_4(\cos\beta)\rangle$ found earlier from fitting the experimental data with Eq. (3). The values obtained were: $A = 0.0017$, $\lambda_2 = -0.91$ and $\lambda_4 = -4.8$. The ODF could then be plotted (Fig. 6(a)) and used to create a histogram of probability of SWNT orientations within the deposited line (Fig. 6(b)). From the ODF it can be calculated that the percentage of SWNTs lying within 30° of the direction of the line is 98%.

The experimental results from the crossed polarisation configuration were treated in a similar way using the following equation:

$$\frac{I_\perp(\theta)}{I_\perp(\theta=0°)} \propto \frac{\langle P_4(\cos\beta)\rangle[-\cos^4\theta+\cos^2\theta-4/35]+\langle P_2(\cos\beta)\rangle/21+1/15}{-\langle P_4(\cos\beta)\rangle 4/35+\langle P_2(\cos\beta)\rangle/21+1/15} \quad (9)$$

analogous to Eq. (3). The order parameters $\langle P_2(\cos\beta)\rangle$ and $\langle P_4(\cos\beta)\rangle$ were determined to be 0.7 and 0.3 respectively, giving ODF parameters of $A = 0.0015$, $\lambda_2 = -5.2$ and $\lambda_4 = 0$. Thus, according to these measurements, the percentage of SWNTs lying within 30° of the direction of the written line was 86%.

The polarised Raman measurements were repeated four more times and the results treated as described in each case. Table I gives the ODF parameters obtained from each experiment. It is clear from repeated experiments that there is a high degree of alignment afforded to the SWNTs deposited by FPN.

After the polarised Raman measurements described above, the sample was rinsed in water: 40 hours of immersion in a water bath at room temperature with no agitation, followed by 20 hours at 50 °C with gentle stirring.

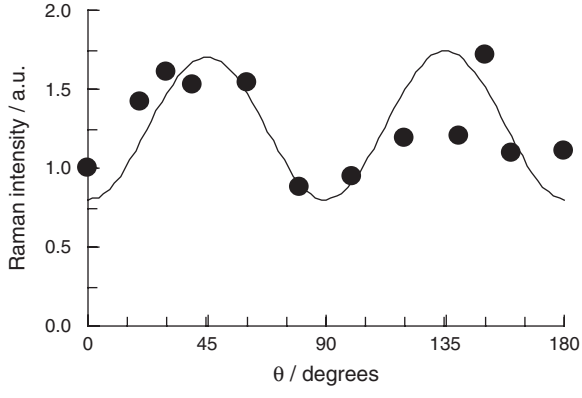

Fig. 7. Intensity of crossed polarisation Raman scattering as a function of θ. The solid line represents a least squares fit based on Eq. (9).

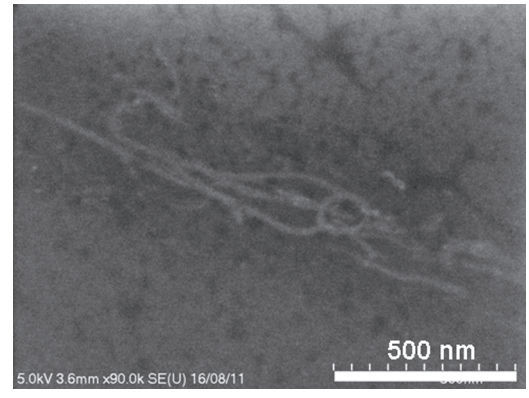

Fig. 8. High-resolution SEM image showing bundles of SWNTs mainly lying in the same direction as the overall deposited line (the darker shadow running from bottom-right to top-left).

AFM scanning revealed an 80% decrease in the height of the lines while the width was unchanged. High-resolution SEM was then able to show bundles of SWNTs inside the written lines (Fig. 8), still with some surfactant present. The alignment of the SWNTs visible in the SEM images is concurrent with the alignment results from the polarised Raman spectroscopy.

The alignment can be considered to be a consequence of the strong interaction of the CNTs with the underlying functionalised substrate combined with the large aspect ratio of the nanotubes, with lengths much longer than the width of the pipette. The pipette draws the nanotubes along in the direction of writing as they leave the tip. The process is crucially dependent on parameters such as the concentration of the nanotube dispersion, the humidity and the quality of the pipette tip.

4. CONCLUSION

We have shown that fountain pen nanolithography is a practical technique for directly depositing carbon nanotubes onto substrates with very high spatial precision. Atomic force microscopy has permitted the examination of the deposition dimensions. Polarised Raman spectroscopy has confirmed the presence of carbon nanotubes in the deposited lines, indicating a very high degree of alignment, making this a suitable method for directly writing nanotube devices.

Acknowledgments: The authors would like to acknowledge the NANOSPEC project, funded by NanoScience Europe via the National Funding Agencies EPSRC and ISF. EEBC acknowledges financial support from the WCU program of the MEST (R31-2008-000-10057-0). Sebastian Heeg and Stephanie Reich are thanked for valuable discussions about polarised Raman measurements.

References and Notes

1. R. Krupke, F. Hennrich, H. B. Weber, M. M. Kappes, and H. V. Löhneysen; Simultaneous deposition of metallic bundles of single-walled carbon nanotubes using Ac-dielectrophoresis; *Nano Letters* 3, 1019 **(2003)**.
2. A. Vijayaraghavan, S. Blatt, D. Weissenberger, M. Oron-Carl, F. Hennrich, D. Gerthsen, H. Hahn, and R. Krupke; Ultra-large-scale directed assembly of single-walled carbon nanotube devices; *Nano Letters* 7, 1556 **(2007)**.
3. A. Lewis, Y. Kheifetz, E. Shambrodt, A. Radko, E. Khatchatryan, and C. Sukenik; Fountain pen nanochemistry: Atomic force control of chrome etching; *Appl. Phys. Lett.* 75, 2689 **(1999)**.
4. H. Taha, R. S.Marks, L. A. Gheber, I. Rousso, J. Newman, C. Sukenik, and A. Lewis; Protein printing with an atomic force sensing nanofountainpen; *Appl. Phys. Lett.* 83, 1041 **(2003)**.
5. Y. Lovsky, A. Lewis, C. Sukenik, and E. Grushka; Atomic-force-controlled capillary electrophoretic nanoprinting of proteins; *Analytical and Bioanalytical Chemistry* 396, 133 **(2010)**.
6. H. Taha, A. Lewis, and C. Sukenik; Controlled deposition of gold nanowires on semiconducting and nonconducting surfaces; *Nano Letters* 7, 1883 **(2007)**.
7. R. D. Piner, J. Zhu, F. Xu, S. H. Hong, and C. A. Mirkin; Dip-pen nanolithography; *Science* 283, 661 **(1999)**.
8. M. Cardona and G. Güntherodt; Light Scattering in Solids II: Basic Concepts and Instrumentation; Springer, Heidelberg **(1982)**.
9. T. Liu and S. Kumar; Quantitative characterization of SWNT orientation by polarized raman spectroscopy; *Chem. Phys. Lett.* 378, 257 **(2003)**.
10. R. Perez, S. Banda, and Z. Ounaies; Determination of the orientation distribution function in aligned single wall nanotube polymer nanocomposites by polarized Raman spectroscopy; *J. Appl. Phys.* 103, 074302 **(2008)**.

Received: 15 November 2011. Accepted: 24 November 2011.